COMITATO NAZIONALE PER L'ENERGIA NUCLEARE
Laboratori Nazionali di Frascati

LNF-75/20(R)
27 Ottobre 1975

G. Paternò and R. Vaglio: ON THE MAGNETIC FIELD DEPENDENCE OF d.c. JOSEPHSON CURRENT IN TUNNELLING JUNCTIONS. -

Servizio Documentazione
dei Laboratori Nazionali di Frascati del CNEN
Casella Postale 70 - Frascati (Roma)

Laboratori Nazionali di Frascati del CNEN
Servizio Documentazione

LNF-75/20(R)
27 Ottobre 1975

G. Paternò and R. Vaglio(x): ON THE MAGNETIC FIELD DEPENDENCE OF d.c. JOSEPHSON CURRENT IN TUNNELLING JUNCTIONS. -

INTRODUCTION. -

In recent years the Josephson effect in tunnelling junctions has been extensively investigated both for its great interest from the theoretical point of view, and for its stimulating applications.

A powerful mean for analyzing the properties of Josephson junctions is provided by the study of the dependence of the maximum d.c. supercurrent I_1 on the applied magnetic field Be. This dependence is intimately related to the current density distribution in the junction and gives information about the uniformity of the oxide barrier.

In the following we present and analyze I_1 v.s.-Be dependences computed starting from different "simplified" shapes of the current density in the barrier (section I). In section II some experimental details concerning the magnetic field measurements are discussed. In section III, I_1 v.s. Be experimental patterns for different junctions are reported, and a discussion of these data in terms of the analysis developed in section I is given.

I. - THEORY

The d.c. Josephson effect can be described by the following equations[1] (see Fig. 1)

(x) - Istituto di Fisica dell'Università di Palermo.

(1a) $$J_z(x, y) = J_1 \sin \varphi (x, y)$$

(1b) $$\vec{\nabla}_{xy} \varphi (x, y) = \frac{2 \pi d}{\Phi_o} \vec{B}(x, y) \times \vec{n}$$

where $\varphi (x, y)$ is the phase difference between the two superconductors, J_1 is the maximum current density, $\vec{B}$ is the magnetic field, $d = \lambda_{11} + \lambda_{21} + t$ is the effective magnetic thickness, $\Phi_o = 2.07 \times 10^{-7}$ Gauss x cm^2 is the flux quantum and $\vec{n}$ is the unit vector perpendicular to the plane of the junction.

Combining relations (1) with Maxwell's equations we have:

(2) $$\nabla^2_{x, y} \varphi = \frac{1}{\lambda_J^2} \sin \varphi$$

where (CGS units)

$$\lambda_J = \left(\frac{\hbar c^2}{8 \pi e J_1 d} \right)^{1/2}$$

is the Josephson penetration depth. If the junction dimensions are small compared with λ_J, equation 2 becomes: $\nabla^2 \varphi = 0$ then $\vec{\nabla} \varphi = \text{const}$ and from (1b) it follows $\vec{B}(x, y) = \text{const} = Be$. Therefore the self-field produced by the current can be neglected and we have to consider only the external field.

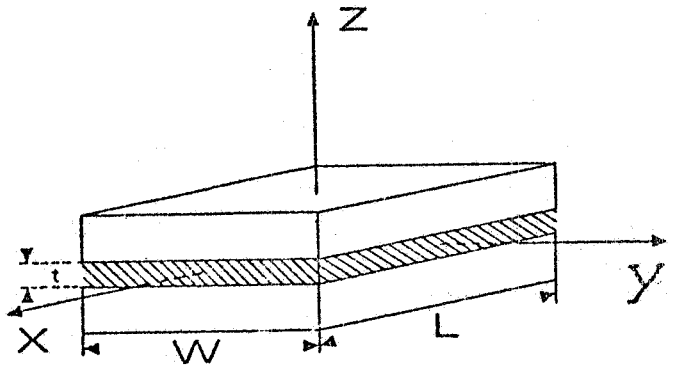

FIG. 1 - Rectangular junction geometry.

In the following we shall consider junctions of rectangular shape (see Fig. 1) whose dimensions (L, W) are less than λ_J; with the external field Be applied in the y direction. In this case to obtain the spatial variation of the phase φ we can integrate equation (1b), and the total current through the barrier is obviously:

$$(3) \qquad I = \int_{-L/2}^{L/2} \int_{-W/2}^{W/2} J(x, y) \sin\left(\frac{2\pi d}{\Phi_o} x + \varphi_c\right) dx\, dy$$

Here the maximum current density J_1 is assumed to be a function of the coordinates in the plane of the junction, to take into account non uniformities of the oxide tunnelling barrier.

Let us define $k = \frac{2\pi d}{\Phi_o} B_e$ and

$$(4) \qquad \mathfrak{J}'(x) = \int_{-W/2}^{W/2} J(x, y)\, dy$$

From (3) it follows:

$$I(k, \varphi_o) = \int_{-L/2}^{L/2} \mathfrak{J}'(x) \sin(kx + \varphi_o)\, dx = \mathrm{Im}\left\{ e^{i\varphi_o} \int_{-L/2}^{L/2} \mathfrak{J}'(x)\, e^{ikx}\, dx \right\}$$

The Josephson current I_1 is obtained taking the maximum with respect to φ_o of this expression.

$$(5) \qquad I_1(k) = \left| \int_{-\infty}^{+\infty} \mathfrak{J}(x)\, e^{ikx}\, dx \right|$$

where $\mathfrak{J}(x) = \mathfrak{J}'(x)$ for $|x| \leq \frac{L}{2}$ and $\mathfrak{J}(x) = 0$ for $|x| > \frac{L}{2}$. Thus, generally, the maximum Josephson current as a function of the applied field is given by the modulus of the Fourier transform of the function $\mathfrak{J}(x)$, and, of course, is strongly connected to the current density profile $J(x, y)$.

Dynes and Fulton[2] have pointed out that it is possible, starting from the I_1 v. s. k pattern, to construct the function $\mathfrak{J}(x)$. However this is not easy to do and, in order to have a good resolution, extremely careful measurements also at high fields, are required where as we will see later, the Josepshson current becomes strongly reduced. In any case one can get only information about $\mathfrak{J}(x)$ which is the integral in the direction of the applied field of the physically interesting quantity $J(x, y)$. Also as remarked by Zappe[3] the procedure of finding $\mathfrak{J}(x)$, starting from I_1 v. s. k pattern doesn't lead to a unique solution unless of specifying some properties of the unknown function $J(x, y)$. Therefore we have found useful to proceed in the

opposite direction: we start from simple current density profiles which seems to be realistic from a physical point of view and we compute from (5) the magnetic field pattern in each case. The experimental data can be qualitatively interpreted by comparison with the computed ones. It is also possible, in particular cases, by varying the parameters which characterize J(x, y) to get a satisfactory quantitative fitting of the experimental pattern and so to obtain more detailed information on the shape of the barrier.

a) - Uniform current density profile. -

Let us start considering the simple case of a uniform barrier $J(x, y) = \text{const} = J_1$

It follows from (4)

$$\mathcal{J}(x) = J_1 \, W P_{L/2}(x)$$

where

$$P_\tau(x): \begin{cases} = 0; |x| > \tau \\ = 1; |x| \leq \tau \end{cases}$$

from (5) it follows that the total current is[4]:

$$(6a) \qquad I_1(k) = J_1 W \left| \int_{-\infty}^{+\infty} P_{L/2}(x) \, e^{ikx} \, dx \right| = I_1(0) \left| \frac{\sin k \frac{L}{2}}{k \frac{L}{2}} \right|$$

where $I_1(0) = J_1 WL$.

Equation (6a) can be rewritten as:

$$(6b) \qquad I_1(\Phi/\Phi_o) = I_1(0) \left| \frac{\sin \pi \, \Phi/\Phi_o}{\pi \, \Phi/\Phi_o} \right|$$

$\Phi = B_e Ld$ is the flux through the junction.

This is the well known Fraunhofer pattern.

Equation (6b) is plotted in Fig. 2. Numerical values of $I_1/I_1(0)$ v. s. Φ/Φ_o are also reported in Table I. The minima ($I_1 = 0$) of the pattern occur at $k(L/2) = n\pi$, $\Phi = \Phi_o$). The distance between the zeros of the central peak is twice that of the secondary peaks. The first maximum is 0.217 of the central one. The secondary maxima decrease rapidly to 0.

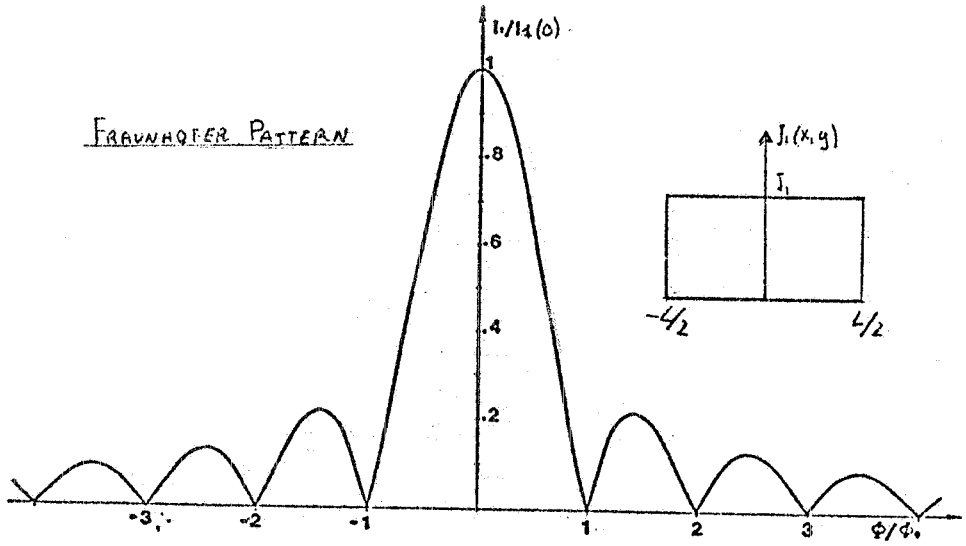

FIG. 2 - $I_1/I_1(0)$ v.s. Φ/Φ_0 rectangular geometry, uniform current density distribution. (Fraunhofer pattern).

b) - "Step-like" current density profile.-

Let us assume now for the current density J(x, y) a step-like profile such as that of Fig. 3. (J is constant in the y direction). It follows:

$$\mathcal{J}(x) = J_1 W \left[\xi P_{1/2}(x) + P_{s/2}(x - \frac{1+s}{2}) + P_{s/2}(x + \frac{1+s}{2}) \right]$$

the meaning of ξ and s is clear from Fig. 3 and $1 = L-2s$.

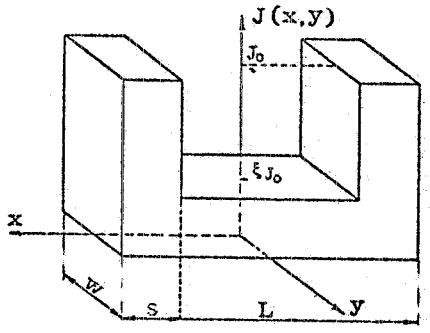

FIG. 3 - Step-like current density distribution.

The maximum current is thus:

$$I_1(k) = J_1 WL \left| \xi \frac{1}{L} \frac{\sin k\frac{1}{2}}{k\frac{1}{2}} + 2\frac{s}{L} \frac{\sin k\frac{s}{2}}{k\frac{s}{2}} \cos \frac{k(L-s)}{2} \right| \quad (7)$$

$$I_1(0) = J_1 WL \left(\xi \frac{1}{L} + 2\frac{s}{L} \right)$$

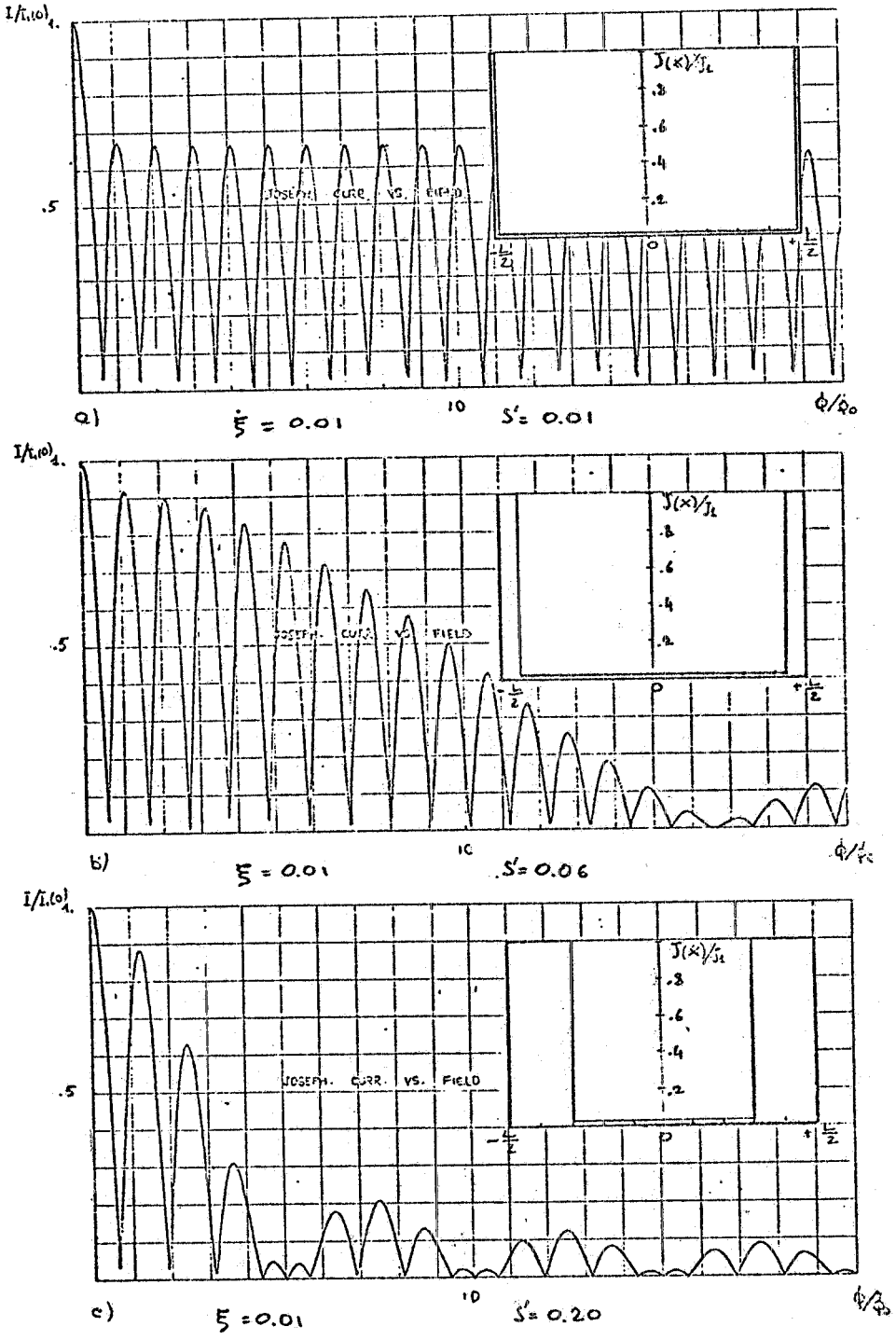

FIG. 4 - $I/I_1(0)$ v.s. Φ/Φ_0 for rectangular junction geometry and a step-like current density distribution.

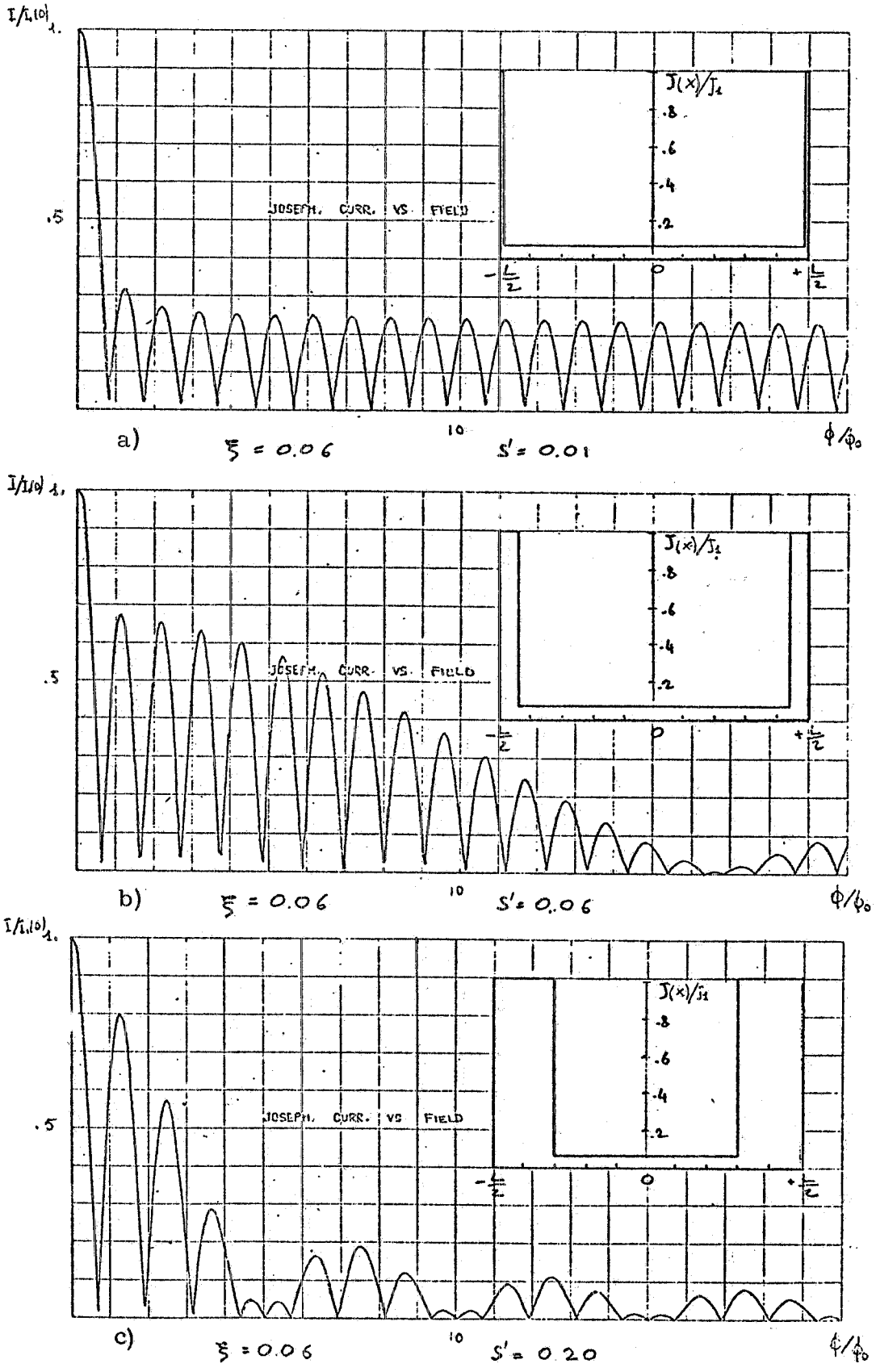

FIG. 5 - $I/I_1(0)$ v.s. Φ/Φ_0 for rectangular junction geometry and a step-like current density distribution.

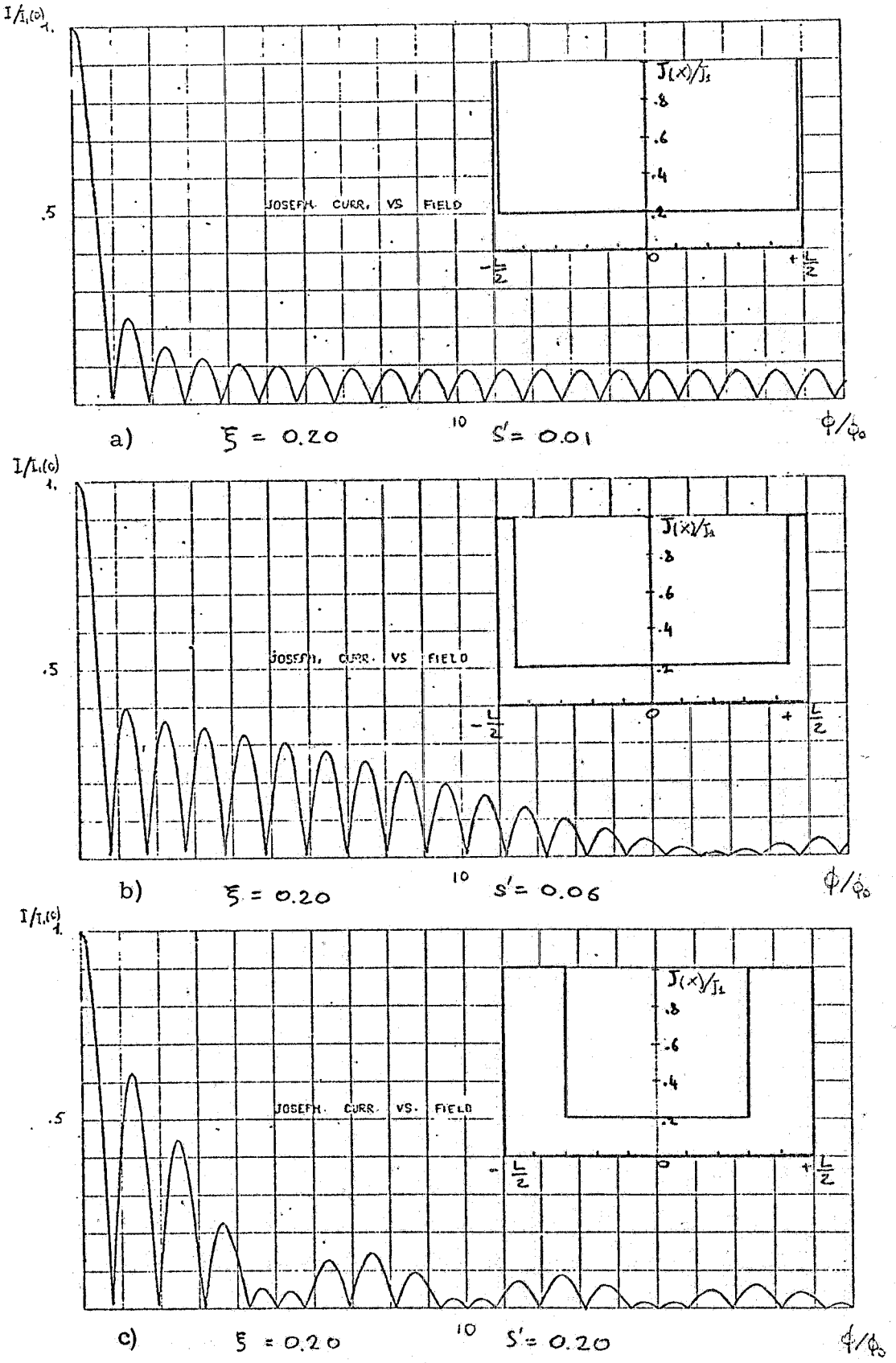

FIG. 6 - $I/I_1(0)$ v.s. Φ/Φ_0 for rectangular junction geometry and a step-like current density distribution.

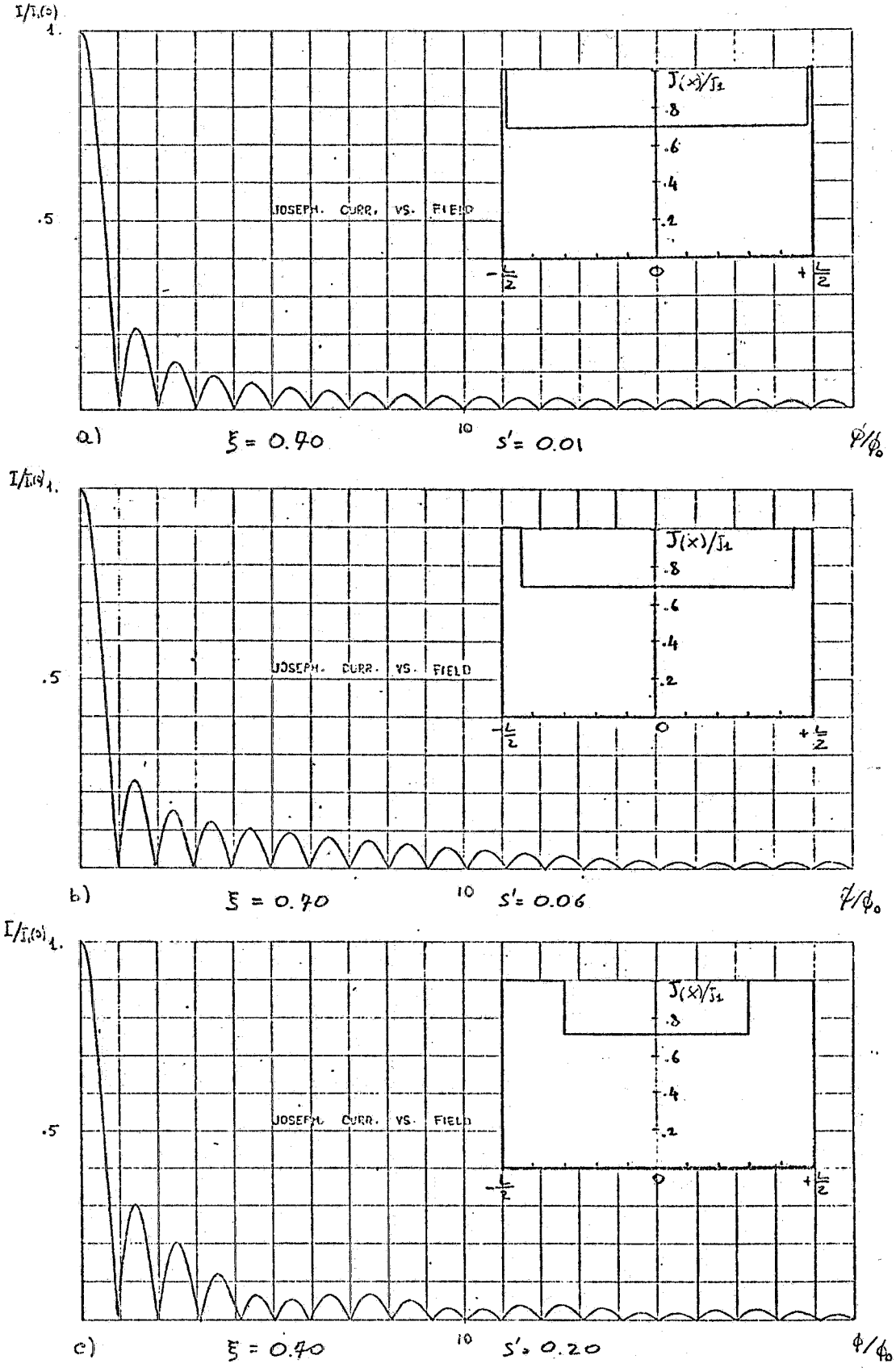

FIG. 7 - $I/I_1(0)$ v. s. Φ/Φ_0 for rectangular junction geometry and a step-like current density distribution.

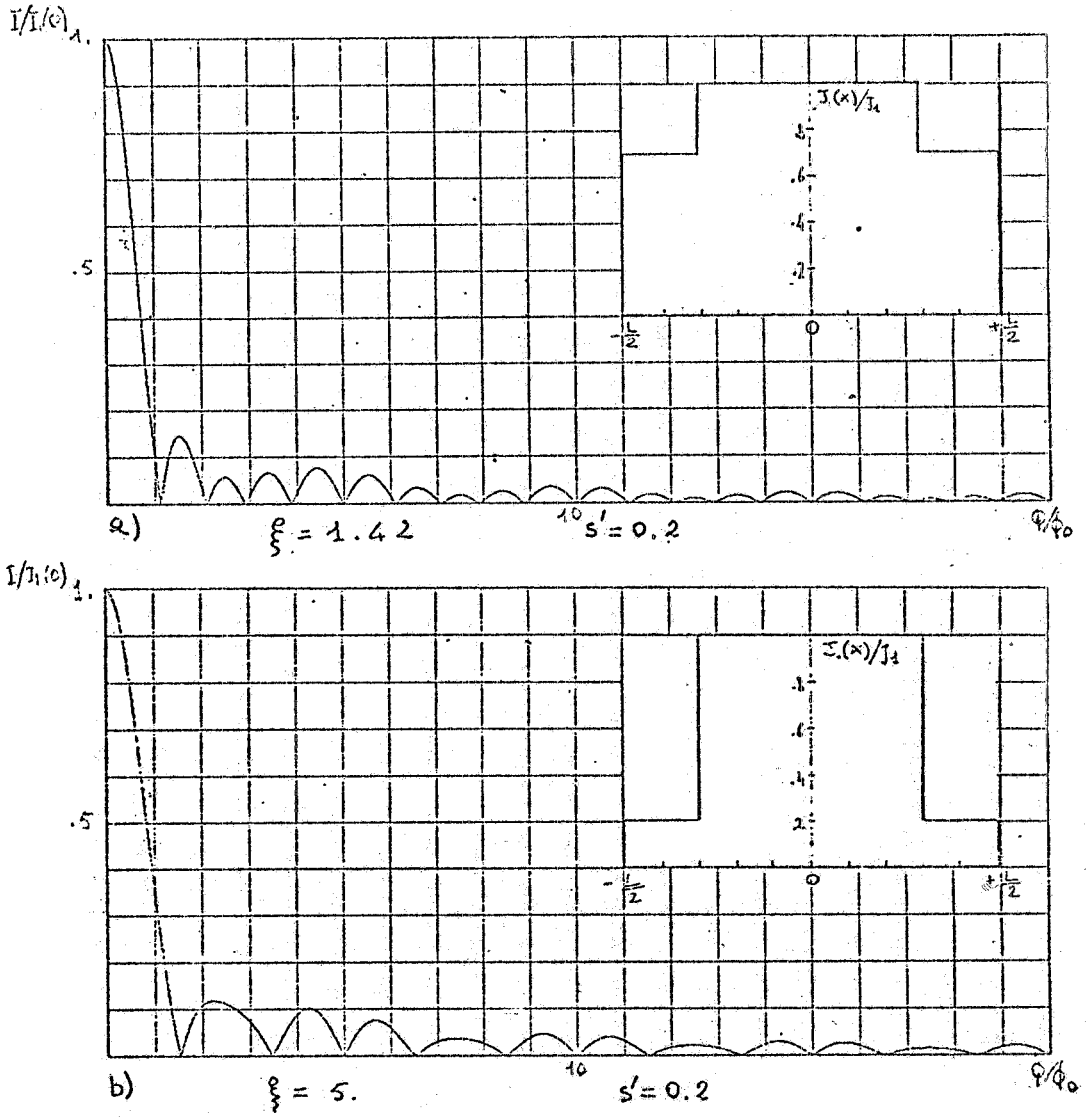

FIG. 8 - $I/I_1(0)$ v.s. Φ/Φ_0 for rectangular junction geometry and a step-like current density distribution.

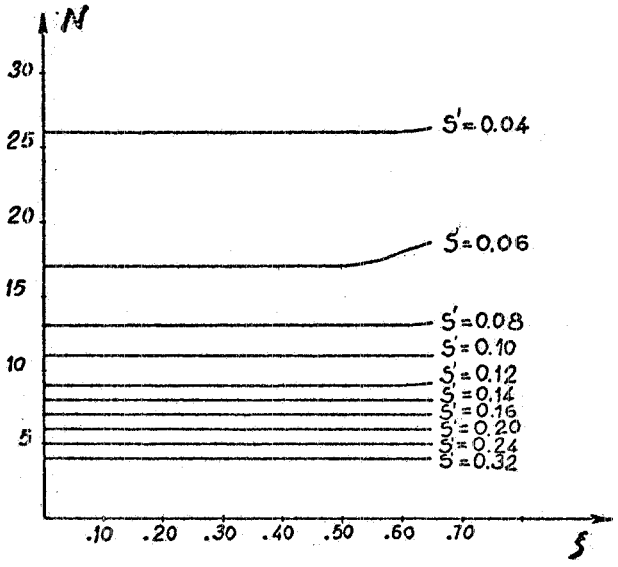

FIG. 9 - Number of maxima N in the first envelope v. s. ξ and s', for I_1 v. s. k patterns of a rectangular junction, with step like current density distribution.

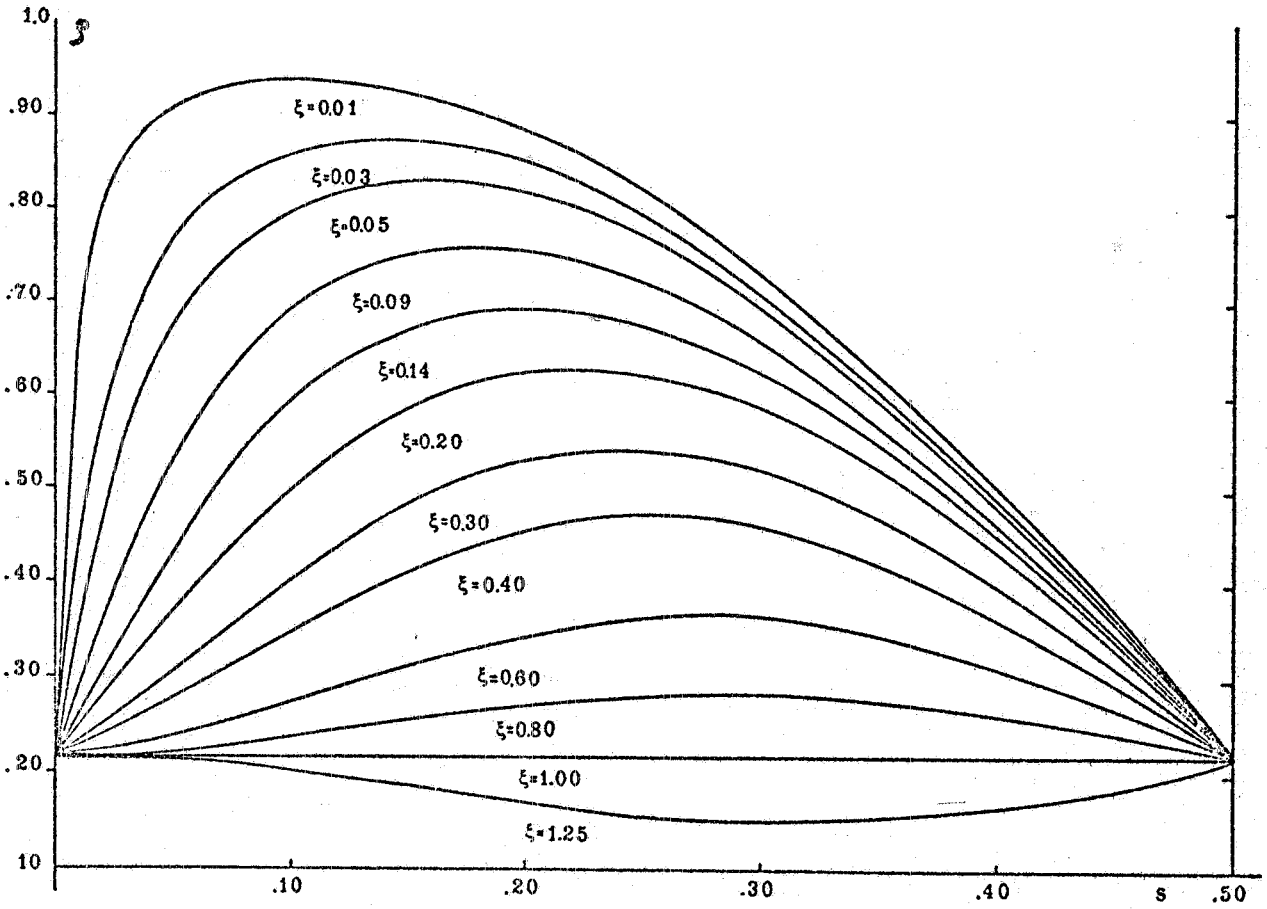

FIG. 10 - Ratio ρ between the first and the central maximum for I_1 v. s. k patterns of a rectangular junction, with steplike current density distribution.

Eq. (7) contains two terms: a Fraunhofer diffraction term whose periodicity is connected with the length 1 of the background current (density ξJ_1), and a "double junction" term which containes a diffraction part related to the dimension s and an interference part whose periodicity is given by the distance L-s between the peaks. Eq. (7) is plotted in Figs. 4-8 for various values of ξ and $s' = s/L$ (Figs. 4-7, $\xi < 1$, Fig. 8, $\xi > 1$). From the analysis of these patterns it can be seen that s is strongly related to the number N of the peaks included in the first envelope of the maxima, whereas ξ gives a measure of the ratio between the central maximum and the secondary ones. This aspect is well clarified in Figs. 9 and 10. In Fig. 9 the number N as a function of ξ is reported for various s' values. It can be seen that for $\xi \lesssim 0.7$ N depends only on s'. In Fig. 10 the ratio ϱ between the first maximum and the central one is reported as a function of s' for various values. It is interesting to see that for $\xi < 1$ we have $\varrho > 0.217$, i.e. a values greater than the one in a simple Fraunhofer pattern, whereas for $\xi > 1$ we have $\varrho < 0.217$. In section III is given an example for the utilization of these diagrams for the determination of s' and ξ.

c) "Exponential" current density profile.-

Let us consider now the current density profile sketched in Fig. 11, whose analytic expression is given by:

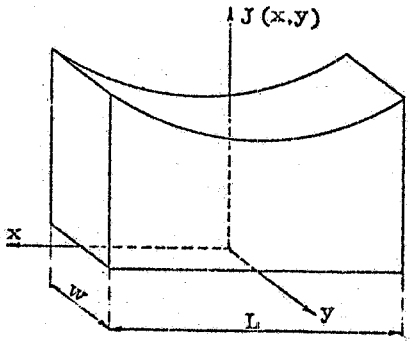

$$J(x, y) = \frac{J_1 \cosh ax}{\cosh \frac{aL}{2}}$$

FIG. 11 - Exponential current density profile.

The parameter a gives a measure of the confinement of the current density at the edges of the junction. We get for the total current in the junction:

$$I_1(k) = \frac{J_1 W}{\cosh a\frac{L}{2}} \left| \int_{-\frac{L}{2}}^{\frac{L}{2}} \cosh ax \, e^{ikx} dx \right|$$

Evaluating the integral:

$$(8a) \qquad I_1(k) = I_1(0) \frac{a^2}{a^2 + k^2} \left| \frac{k}{a} \frac{\sin k\frac{L}{2}}{\tanh \frac{aL}{2}} + \cos k\frac{L}{2} \right|$$

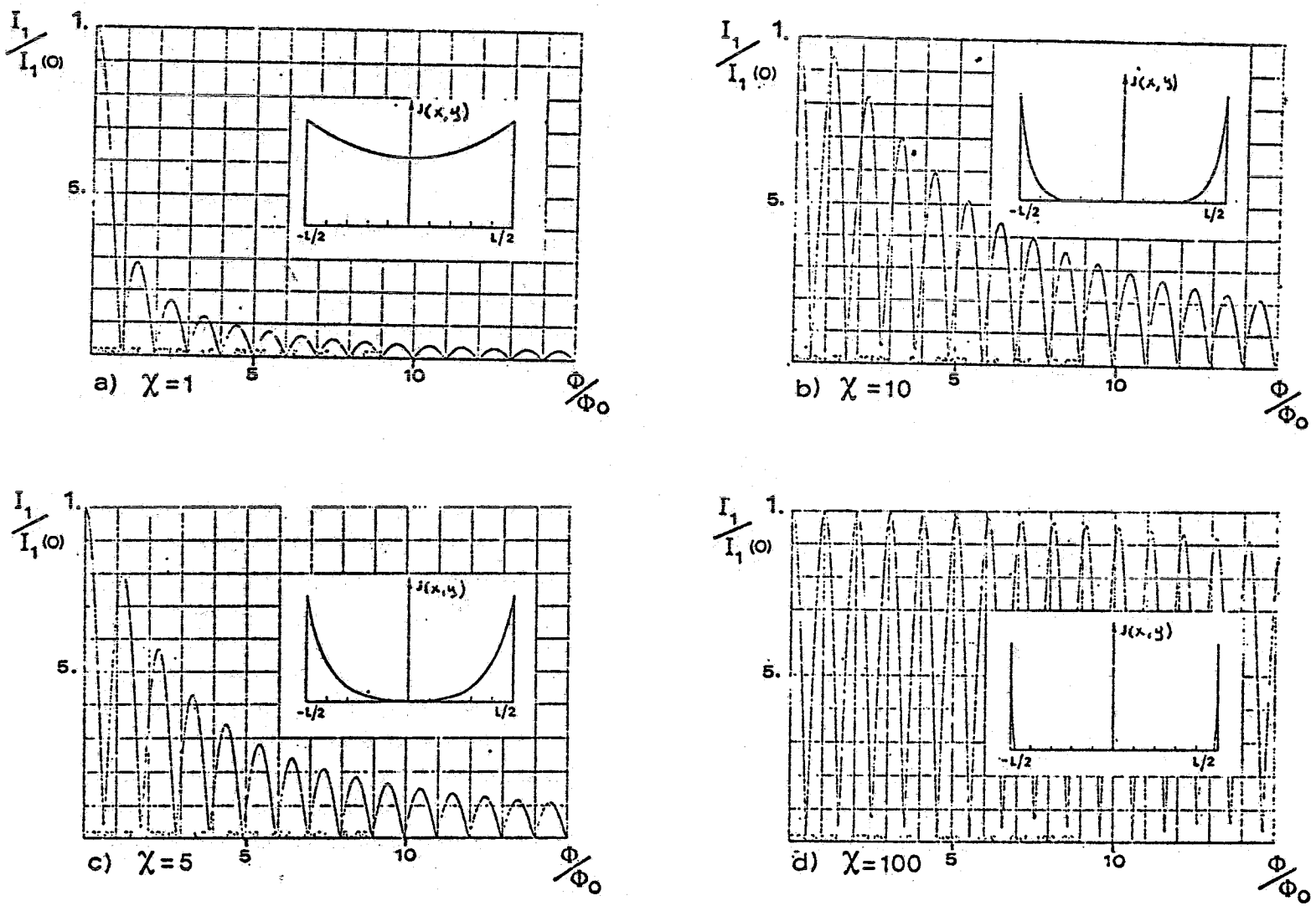

FIG. 12 - $I/I_1(0)$ v. s. Φ/Φ_0 for rectangular junction geometry and an exponential current density distribution.

where:

$$I_1(0) = \frac{2J_1}{a} W \tanh \frac{aL}{2}$$

In terms of the flux in the junction (8a) becomes:

$$(8b) \qquad I_1(\Phi/\Phi_o) = I_1(0) \frac{\chi^2}{\chi^2 + (\frac{\pi\Phi}{\Phi_o})^2} \left| \frac{\pi \frac{\Phi}{\Phi_o} \sin \pi \frac{\Phi}{\Phi_o}}{\chi \tanh \chi} + \cos \pi \frac{\Phi}{\Phi_o} \right|$$

where

$$\chi = \frac{La}{2}$$

This dependence is reported in Fig. 12 for different values of χ. In Fig. 13 the ratio ϱ between the first and the central maximum is plotted as a function of χ.

By equating to zero the expression (8b) it is possible to find the values of Φ at which the minima occur.

We get:

$$\pi \frac{\Phi}{\Phi_o} \tan \pi \frac{\Phi}{\Phi_o} + \chi \tanh \chi = 0$$

In Fig. 14 the first term of this equation is plotted as a function of Φ / Φ_o. The minima are found from the intercept of a straight line corresponding to a given value of the constant χ (and so of $\chi \tanh \chi$) with this curve. As is expected (eq. (8b)) for $\chi \longrightarrow 0$ (uniform current density distribution) the distance between the minima occur as in a Fraunhofer pattern. For $\chi \longrightarrow \infty$ (current completely peaked at the edges) the distance between all the consecutive minima is the same (double junction interference behaviour).

As is clearly apparent from Fig. 14 this one parameter model for the current density profile is very useful to describe the gradual passage from single to double junction behaviour when the current becomes more and more peaked at the edges.

d) Triangular current density profile.-

Let us refer now to the triangular current density profile (see Fig. 15 inset) described by

$$J(x, y) = J_1 q_{L/2}(x) \qquad \text{where} \quad q_{L/2}(x) = \begin{cases} 1 - \frac{2|x|}{L} & |x| \leq \frac{L}{2} \\ 0 & |x| > \frac{L}{2} \end{cases}$$

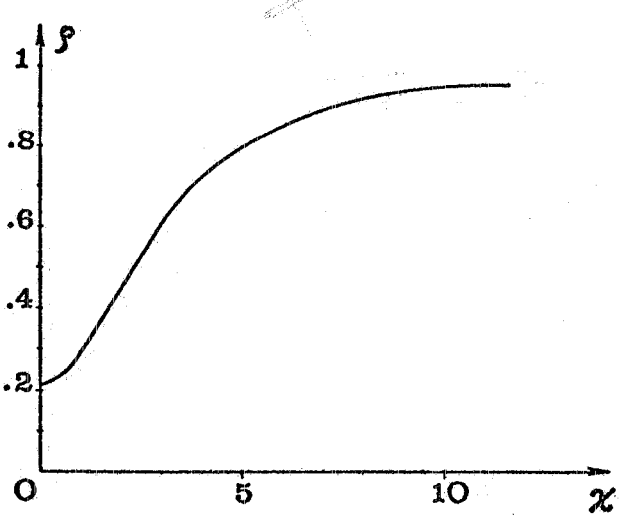

FIG. 13 - Ratio ρ between the first and the central maximum for I_1 v. s. k patterns of a rectangular junction, with exponential current density distribution.

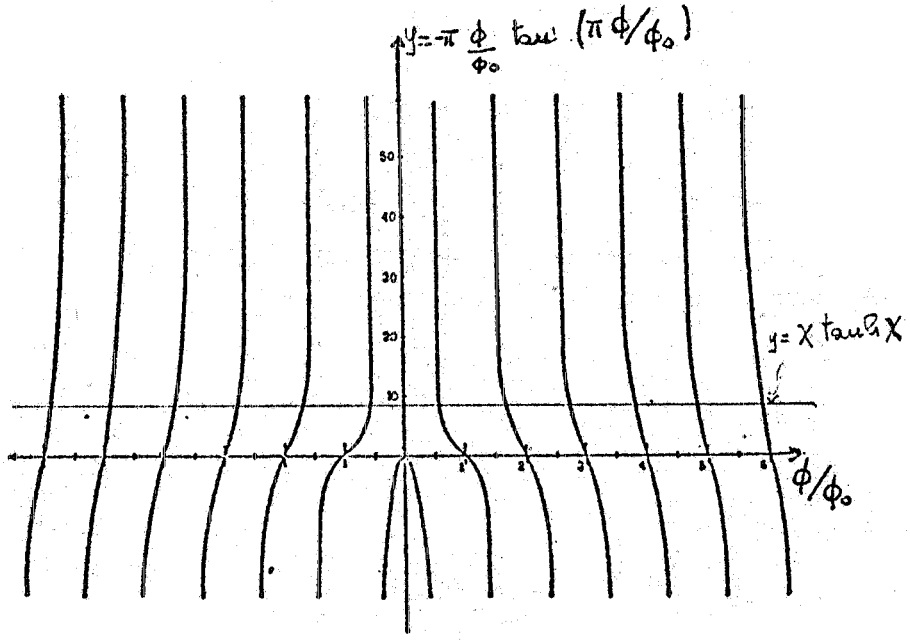

FIG. 14 - Graphical solution of the equation for the minima in the I_1 v. s. k pattern for exponential current density distribution.

in this case:

$$\mathcal{J}(x) = J_1 W q_{L/2}(x)$$

Observing that the derivative of $\mathcal{J}(x)$ is given by:

$$\frac{d}{dx}\mathcal{J}(x) = \frac{2J_1 W}{L}\left[P_{L/4}(x+\frac{L}{4}) - P_{L/4}(x-\frac{L}{4})\right]$$

and that[4] if F(k) is the Fourier transform of f(x), the Fourier transform of $\int_{-\infty}^{x} f(x')\,dx'$ is given by $\frac{F(k)}{ik}$ we obtain for the total current in the junction:

$$I_1(k) = I_1(0)\left\{\frac{\sin k\frac{L}{4}}{k\frac{L}{4}}\right\}^2 \tag{9}$$

where:

$$I_1(0) = \frac{J_1 WL}{2}$$

This expression is also plotted in Fig. 15.

e) "Circular" current density profile.-

Another very interesting current density profile is that reported in the inset of Fig. 16. Its expression is:

$$J(x, y) = \frac{2J_1}{L}\sqrt{\frac{L^2}{4} - x^2}$$

The total current is:

$$I_1(k) = \frac{2J_1 W}{L}\left|\int_{-\frac{L}{2}}^{\frac{L}{2}} \sqrt{\frac{L^2}{4} - x^2}\, e^{ikx}\, dx\right|$$

By the simple substitution $x = L/2 \cos\theta$ we get:

$$I_1(k) = J_1 WL\left|\int_0^{\pi/2} \cos\left(\frac{kL}{2}\cos\theta\right)\sin^2\theta\, d\theta\right|$$

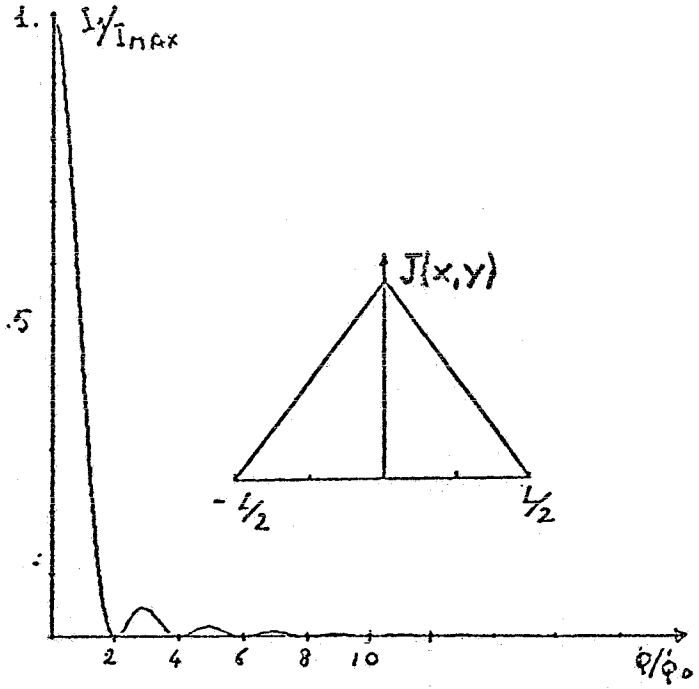

FIG. 15 - $I_1/I_1(0)$ v.s. Φ/Φ_0 for rectangular junction geometry and triangular current density profile.

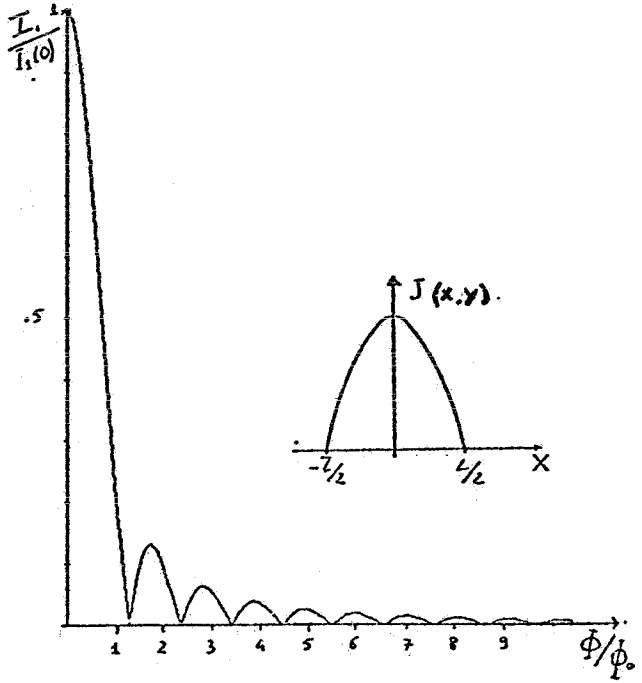

FIG. 16 - $I_1/I_1(0)$ v.s. Φ/Φ_0 for rectangular junction geometry and circular current density profile.

The last integral can be computed[5] in terms of Bessel functions and finally we have:

$$(10) \qquad I_1(\Phi/\Phi_o) = I_1(0) \left| \frac{2 J_1(\pi \frac{\Phi}{\Phi_o})}{\pi \frac{\Phi}{\Phi_o}} \right|$$

$$I_1(0) = \frac{\pi}{4} W L J_1$$

where $J_1(x)$ is the Bessel function of first kind. The expression (10) is plotted in Fig. 16. Numerical values of $I_1/I_1(0)$ v. s. B/B_o, where B_o is the field for which the first minimum occurs, are reported in Table II.

It is interesting to observe that a junction of circular geometry and J = const. leads to an equivalent expression for $\mathcal{J}(x)$ and so to the same I. v. s. k dependence. Let us remark that it is generally possible to obtain the same $\mathcal{J}(x)$ starting from rectangular geometries with non-uniform current densities or from an appropriate geometry with a uniform current distribution.

f) Asymmetric current density profiles.-

Let us consider now two asymmetric current density profiles. The first one is (see Fig. 17).

$$J(x, y) = J_1(1 - \frac{\eta}{2} - \eta \frac{x}{L}) P_{L/2}(x)$$

and therefore

$$(11) \qquad I_1(k) = \left| 2 J_1 W (1 - \frac{\eta}{2}) \frac{\sin k \frac{L}{2}}{k} - i 2 J_1 \frac{W}{L} \eta (\frac{L}{2} \frac{\cos k \frac{L}{2}}{k} - \frac{\sin k \frac{L}{2}}{k^2}) \right|$$

$$I_1(0) = J_1 WL (1 - \eta/2)$$

This expression is plotted for $\eta = 1/3$ in Fig. 17. It is interesting to observe that the current at the minima is not zero and from eq. (11) is given by:

$$I_1(k_n) = J_1 W \eta / k_n$$

where $k_n = 2n\pi/L$ is the value of k at which the n th minimum occurs.

In the second case the current density is (see Fig. 18):

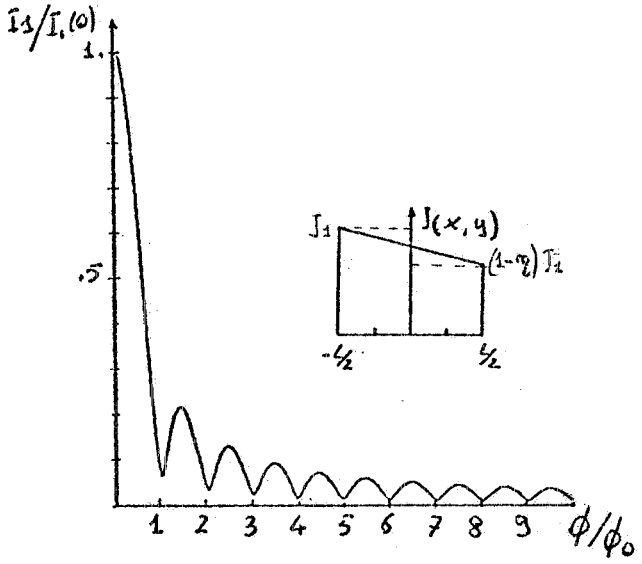

FIG. 17 - $I_1/I_1(0)$ v. s. Φ/Φ_0 for rectangular junction geometry and linear asymmetric current density profile.

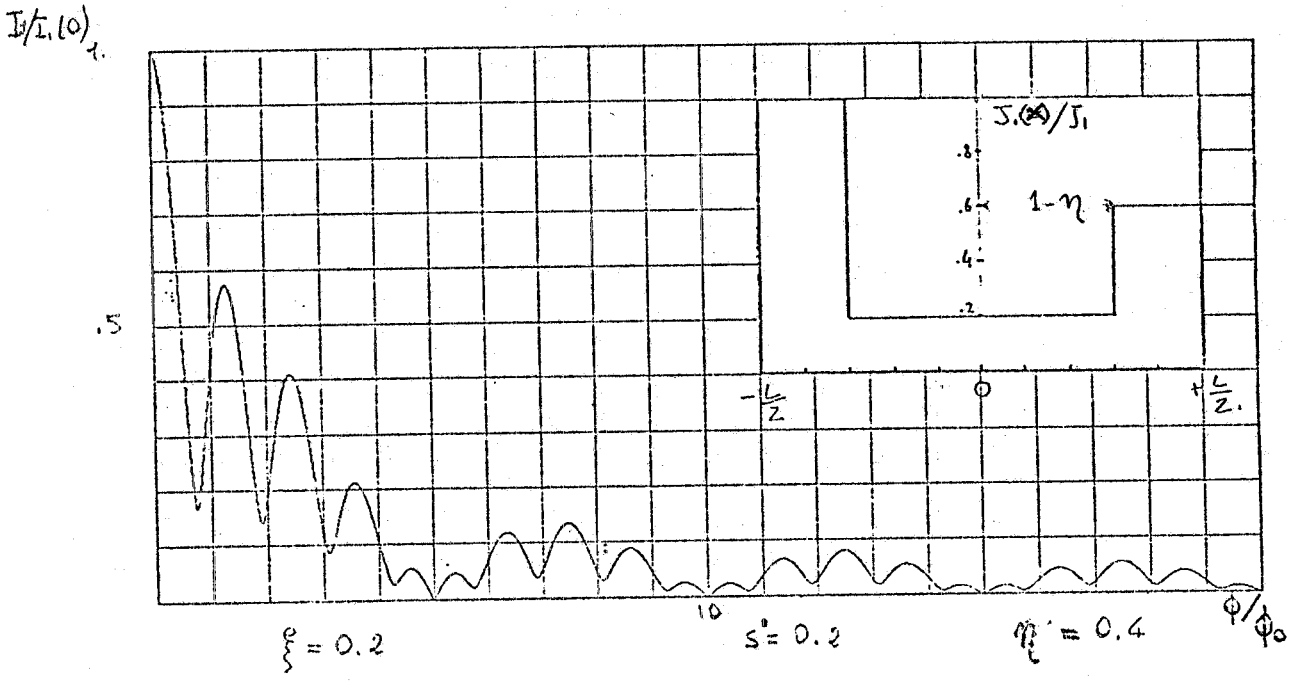

FIG. 18 - $I_1/I_1(0)$ v. s. Φ/Φ_0 for rectangular junction geometry and asymmetric step like current density profile.

$$J(x,y) = J_1 \left[\xi P_{1/2}(x) + P_{s/2}(x - \frac{1+s}{2}) + P_{s/2}(x + \frac{1+s}{2}) - \eta P_{s/2}(x - \frac{1+s}{2}) \right]$$

From this expression it follows, for the total current:

$$I_1(k) = J_1 WL \Big| \xi \frac{1}{L} \frac{\sin k\frac{1}{2}}{k\frac{1}{2}} + \frac{s}{L}(2+\eta) \frac{\sin k\frac{s}{2}}{k\frac{s}{2}} \cos k \frac{(L-s)}{2} +$$

$$(12) \qquad - i\eta \frac{s}{L} \frac{\sin k\frac{s}{2}}{k\frac{s}{2}} \sin k \frac{(L-s)}{2} \Big|$$

$$I_1(0) = J_1 WL \left[\xi \frac{1}{L} + (2+\eta) \frac{s}{L} \right]$$

This expression is plotted in Fig. 18 for $\eta = 0.4$, $\xi = 0.2$, $s' = 0.2$.

Also in this case the current at the minima is different from 0.

At this point we can draw some general conclusions on the I_1 v. s. B_e behaviour of junctions with non uniform current density distribution.

i) Referring to the Fraunhofer pattern we can say that current densities peaked at the edges produce an increase of the ratio ϱ between the first maximum and the central one (see Figs. 5-6-7-12-18). In this case we observe also that the first minimum occurs for $\Phi/\Phi_0 < 1$

ii) Current density profiles peaked at the center of the junction, give rise to a decrease of the ratio ϱ (see for example Figs. 8-15-16). Furthermore the first minimum occurs for $\Phi / \Phi_0 > 1$.

iii) Double modulation effects can be accounted assuming a step-like profile (see Figs. 4-8).

iiii) Single or double junction behaviour is well characterized by the width of the central peak of the magnetic pattern compared to the other ones (Fig. 14).

iiiii) Asymmetries in the current density profiles lead to non-zero minima in I_1 v. s. B_e curves (see Figs. 17-18).

g) Non parallel magnetic field.-

All these considerations are valid only for fields parallel to one dimension of the junction. Let us suppose now that the external field B_e has also an x component different from zero: if α is the angle between B_e and the y direction we have

(13) $$B_x = B_e \sin\alpha\,; \quad B_y = B_e \cos\alpha\,; \quad B_z = 0$$

For a rectangular junction with a uniform current density distribution we have for the total current:

(14) $$I_1 = J_1 WL \left| \frac{\sin \pi \frac{\Phi_x}{\Phi_o}}{\pi \frac{\Phi_x}{\Phi_o}} \right| \left| \frac{\sin \pi \frac{\Phi_y}{\Phi_o}}{\pi \frac{\Phi_y}{\Phi_o}} \right|$$

where

$$\Phi_x = W.d\,B_x \quad \text{and} \quad \Phi_y = L\,d\,B_y$$

It is useful to have the last expression in terms of B_e. In fact this is generally the quantity measured in the experiments by monitoring the current in the coils that produce the field.

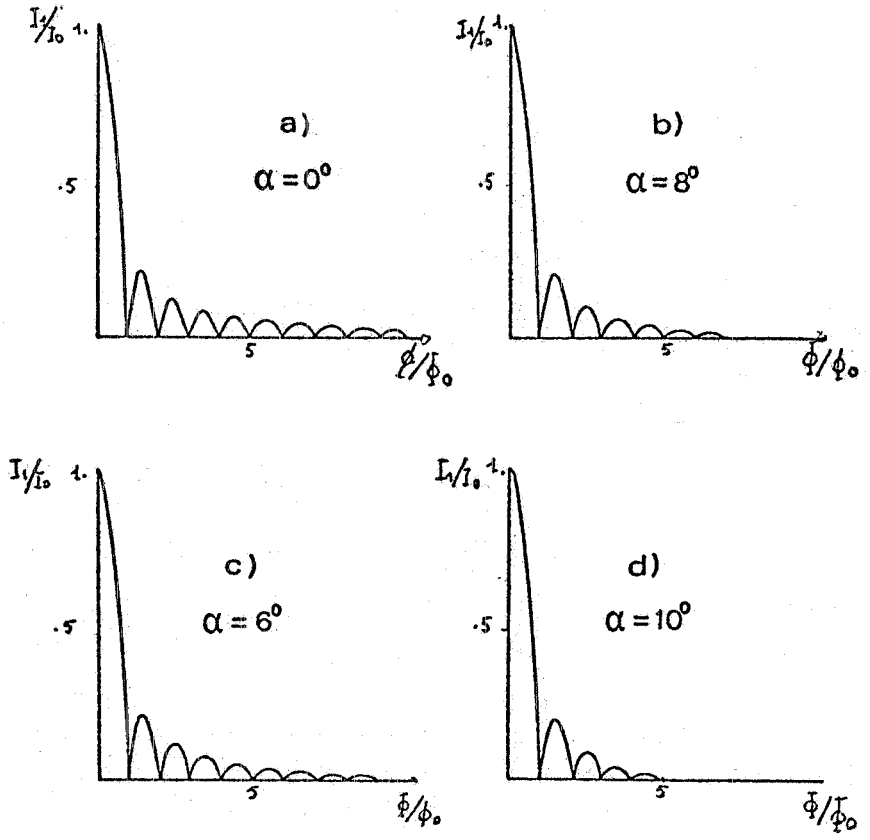

FIG. 19 - $I_1/I_1(0)$ v. s. Φ/Φ_o for non parallel magnetic field.

From (13) and (14) we have

$$(15) \qquad I_1(\Phi/\Phi_o) = I_1(0) \left| \frac{\sin \pi \frac{\Phi}{\Phi_o} \cos\alpha}{\pi \frac{\Phi}{\Phi_o} \cos\alpha} \right| \left| \frac{\sin \pi \frac{\Phi}{\Phi_o} \frac{W}{L} \sin\alpha}{\pi \frac{\Phi}{\Phi_o} \frac{W}{L} \sin\alpha} \right|$$

where

$$\Phi = L\, dB_e$$

Expression (15) is plotted in Fig. 19 for $W/L = 1$ and for various values of the angle α.

It is evident the progressive depression of the secondary maxima.

II. - EXPERIMENTAL DETAILS. -

In this section we will describe the experimental apparatus for measuring I_1 v. s. B_e patterns on Josephson tunnel junctions. The magnetic field is generated by a solenoid whose characteristic are:

Length = 120 mm
Diameter = 40 mm
Total number of turns 7936, on 10 sheets
Copper wire 0.12 mm ϕ
The resistence is about 14 Ω at T 4.2°K
The magnetic field produced is: $B_e = 0.79$ Gauss/mA

Alternatively the field can be produced by a couple of Helmotz coils whose characteristics are:

Internal diameter 40 mm
Distance between coils 19 mm
Number of turns for each coil 441 (21 turns x 21 sheets)
Copper wire 0.10 mm ϕ
The magnetic field produced is $B_e = 0.16$ Gauss/mA.

Of course in this case the field is less uniform. In both cases the coils are located around the sample directly in the helium bath.

In our junctions the field necessary to depress to zero the Josephson current is of the order of few Gauss and so the earth's field is a strong perturbation to the measurements. To achieve a good shielding of the ambient magnetic field the apparatus is surrounded by a cylindrical lead shield, coaxial with the solenoid and closed at the bottom (60 mm Φ x 240 mm length) which acts by excluding the magnetic field via the Meissner effect.

It is important to remark that the field produced inside the coil will be reduced by the superconducting currents induced on the surface of the shield. The effective field can be expressed as:

$$B_{eff} = B_s \left(1 - \frac{r^2}{R^2}\right) \tag{16}$$

where B_s is the field produced by the solenoid and r and R are the radii of the solenoid and of the superconducting shield respectively. We have measured the ratio B_{eff}/B_s directly by performing two runs of measurements on the same junction with and without the shield (see Fig. 20). The two magnetic patterns differ only by a scale factor on the field axis of 0.59 ± 0.02 (in good agreement with that computed from (16)).

The sample holder with the solenoid and the lead shield is shown in Fig. 21.

To reduce further the ambient field and to avoid the possibility of flux trapping in the superconducting shield the cryostat is surrounded by two coaxial μ-metal cylindrical cans. Their dimensions are:

External shield:	thickness	1 mm
	diameter	320 mm
	length	900 mm
Internal shield	thickness	1 mm
	diameter	260 mm
	length	500 mm

The theoretical shielding factors that we obtain (ref. (6)) assuming $\mu \simeq 30.000$ are

Transversal screening factor $S_T \simeq 3.000$
Longitudinal screening factor $S_L \simeq 600$

The maximum d.c. Josephson current is measured following the technique described in ref. (7)(8).

The field is measured by monitoring the current in the solenoid. The I_1 v.s. B_e pattern can be obtained point by point, or directly on an X-Y recorder.

A typical direct recording of an experimental I_1 v.s. B_e pattern is shown in Fig. 22.

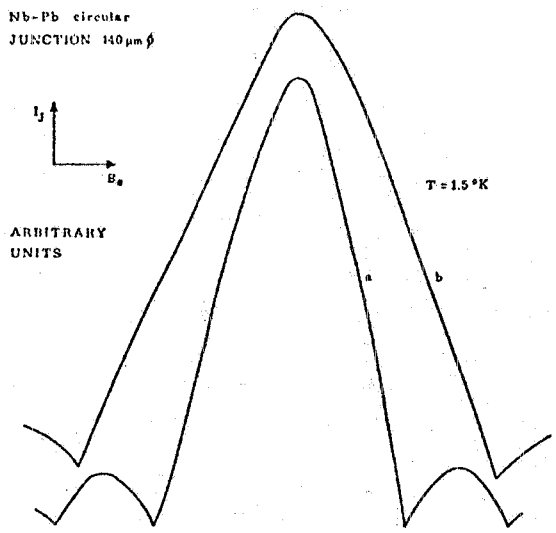

a) I_J vs Be curve withot the screen

b) I_J vs Be curve with the screen

FIG. 20 - Effect of the superconducting shield.

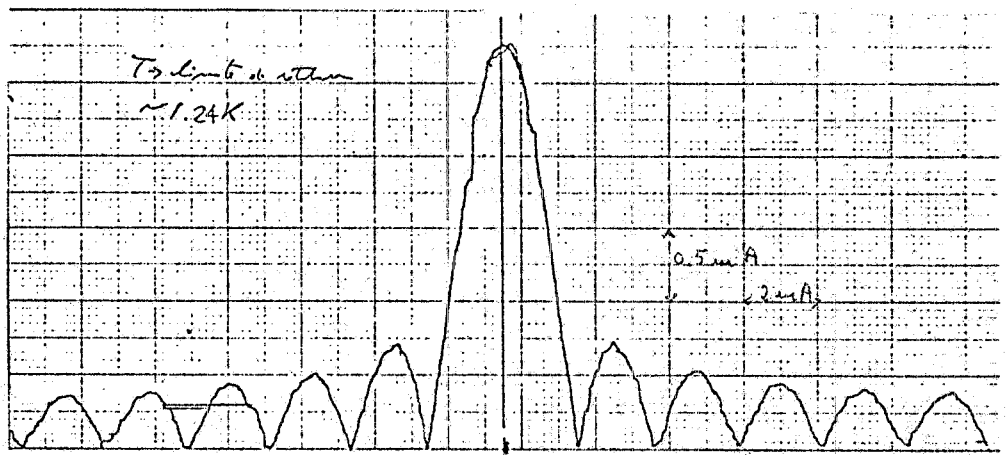

FIG. 22 - Typical direct recording of an experimental I v.s. B_e pattern.

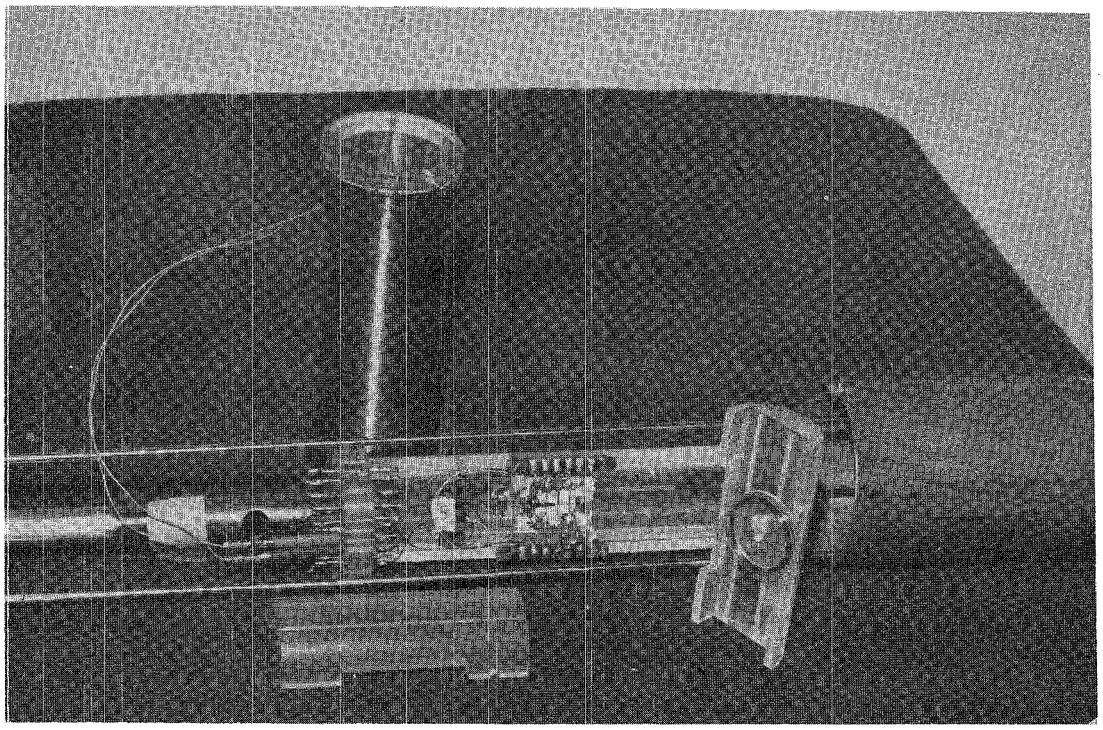

Fig. 21

III. - EXPERIMENTAL RESULTS: ANALYSIS. -

In this section we present some experimental I_1 v. s. B_e patterns and we discuss them in terms of the analysis developed in Section I. All the experiments were carried out using the apparatus described in the previous section. We will refer always to "cross--type" thin film Josephson tunnel junctions deposited on 3/4 "x1" glass substrates. Typical critical currents of our samples were on the order of few mA. The field is generally parallel to the first-deposited strip.

Measurements on a S_n-S_n square junction (0.20×0.20 mm^2) are reported in Fig. 23a. As we can see this pattern presents a double modulation effect and we have fitted it with a step-like current density distribution.

The number N of the peaks in the first envelope of the maxima is about 10. From Fig. 9 this gives for s' the value $s' \simeq 0.11$. The mean values of the ratio between the central peak and the two adjacent ones, is $\varrho \simeq 0.8$. This gives, using Fig. 10, $\xi \simeq 0.06$. The theoretical pattern computed using the step-like current density profile corresponding to these values of ξ and s', is reported in Fig. 23a. In the same Fig. 23 is also reported a sketch of the current density profile used.

As we can see, all the essential features of the experimental pattern are well reproduced. This kind of pattern is often observed in experiments: in fact a strong enhancement of the current density in cross type junction can be due to shorts at the edges of the bottom film. This effect can be easily verified observing that a I_1 v. s. B_e pattern measured with the field along the direction of the top film, often gives an ordinary Fraunhofer-like pattern.

It is interesting also to observe that the characteristic higher value of the central peak referred to the envelope of the secondary ones is associated with the small background current over the whole junction.

Measurements on an N_b-P_b junction (0.20×0.50 mm^2) of cross--type geometry are reported in Fig. 24a. Owing to the absence of double modulation and to the higher value of the first maximum (compared to the Fraunhofer pattern), we have used a current density profile like that of Fig. 11. The ratio ϱ between the first and central maximum is $\varrho \simeq 0.4$. This gives (from Fig. 13) $\chi \simeq 1.75$ (Fig. 24b, inset). The theoretical pattern corresponding to this value is plotted in Fig. 24b.

Finally we report a careful fitting of the experimental results of Fig. 22. Measurements refer to a S_n-S_n cross-type junction (0.18×0.37 mm^2). In this case the best theoretical curve has been obtained

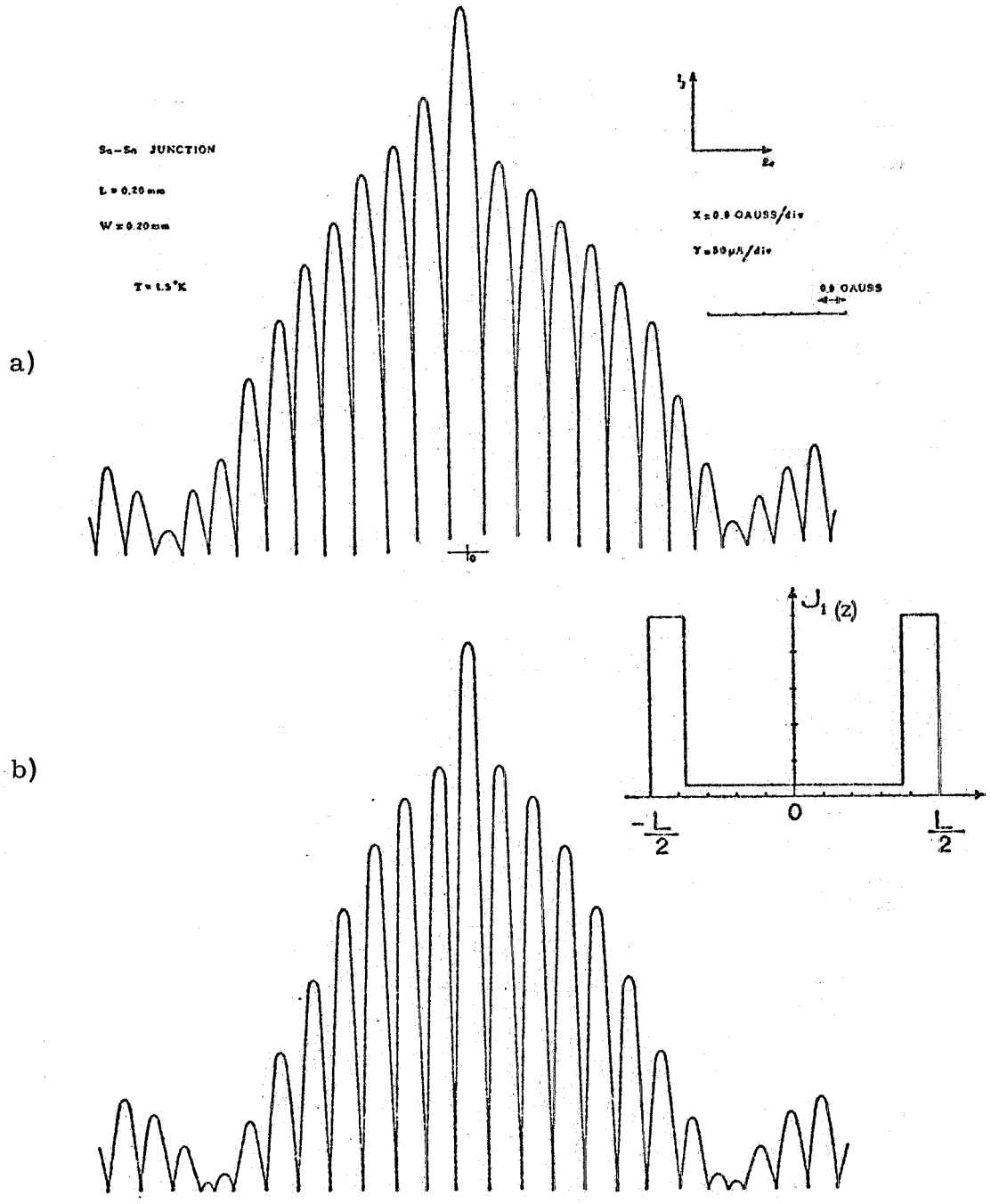

FIG. 23 - I_1 v. s. B_e for a S_n-$S_{n_x}O_y$-S_n "cross type" junction (0.20 mm x 0.20 mm): a) experimental pattern, b) theoretical pattern computed with the current density profile in the inset.

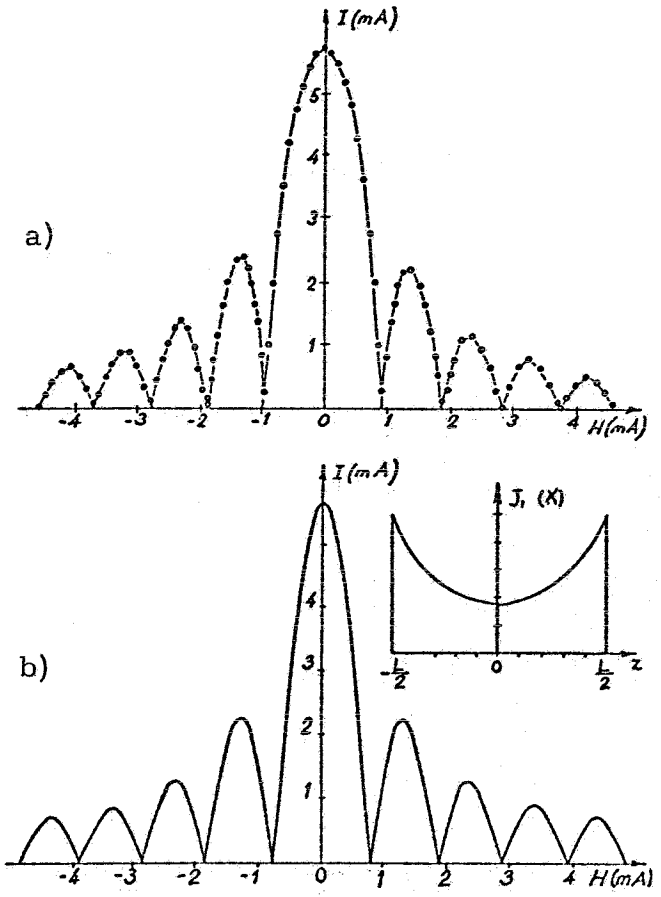

FIG. 24 - I_1 v.s. B_e for a Nb-Nb_xO_y-Pb "cross type" junction (0.20 mm x 0.50 mm): a) experimental pattern, b) theoretical pattern computed with the current density profile in the inset.

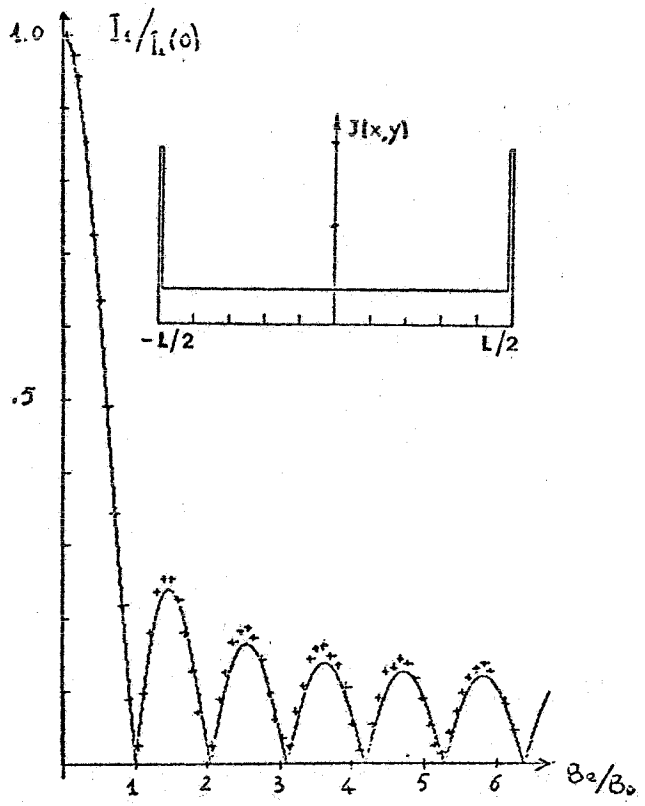

FIG. 25 - Sn-Sn_xO_y-Sn junction (0.18 mm x x 0.37 mm). The crosses are the experimental points).

using a step-like current density profile starting from approximate values of ξ and s', determined with the procedure described above, and then adjusting them, by a computer program, to minimize the sum of the square differences between the experimental and the theoretical values. The results of this analysis are reported in Fig. 25 (the crosses are the experimental points). The best fitting parameters are $\xi = 0.18$ and $s' = 0.012$.

ACKNOWLEDGEMENTS. -

The authors are grateful to Prof. A. Barone, Prof. R. D. Parmentier, M. La Rovere and C. Salvia.

REFERENCES. -

(1) - B. D. Josephson, Adv. Phys. 14, 419 (1965).
(2) - R. C. Dynes and T. A. Fulton, Phys. Rev. B3, 3015 (1971).
(3) - H. H. Zappe, Phys. Rev. B11, 2535 (1975).
(4) - A. Papoulis, The Fourier integral and its Applications (McGraw-Hill, New York, 1962).
(5) - J. Matisoo, J. Appl. Phys. 40, 1813 (1969).
(6) - A. J. Mager, IEEE Trans. on Magnetics 6, 67 (1970).
(7) - E. P. Balsamo, A. Barone, G. Paternò, P. Rissman and M. Russo, Phys. Rev. B10, 1881 (1974).
(8) - K. Baker, E. P. Balsamo, A. Barone e G. Paternò, Report LNF-75/17(R) (1975) (In Italian).

TABLE I

Fraunhofer pattern for a rectangular junction.

$B/B_o^{(x)}$	$I/I_1(0)$	B/B_o	$I/I_1(0)$	B/B_o	$I/I_1(0)$	B/B_o	$I/I_1(0)$
0.05	0.99589	2.55	0.12329	5.05	0.00985	7.55	0.04164
0.10	0.98363	2.60	0.11644	5.10	0.01027	7.60	0.03984
0.15	0.96340	2.65	0.10703	5.15	0.02805	7.65	0.03708
0.20	0.93549	2.70	0.09538	5.20	0.03597	7.70	0.03345
0.25	0.90032	2.75	0.08186	5.25	0.04286	7.75	0.02905
0.30	0.85839	2.80	0.06683	5.30	0.04858	7.80	0.02400
0.35	0.81033	2.85	0.05072	5.35	0.05301	7.85	0.01842
0.40	0.75683	2.90	0.03393	5.40	0.05606	7.90	0.01247
0.45	0.69865	2.95	0.01689	5.45	0.05768	7.95	0.00628
0.50	0.63662	3.00	0.00001	5.50	0.05788	8.00	0.00001
0.55	0.57162	3.05	0.01631	5.55	0.05665	8.05	0.00617
0.60	0.50455	3.10	0.03172	5.60	0.05406	8.10	0.01213
0.65	0.43633	3.15	0.04587	5.65	0.05020	8.15	0.01772
0.70	0.36789	3.20	0.05846	5.70	0.04519	8.20	0.02281
0.75	0.30011	3.25	0.06925	5.75	0.03915	8.25	0.02727
0.80	0.23387	3.30	0.07803	5.80	0.03227	8.30	0.03102
0.85	0.17001	3.35	0.08466	5.85	0.02472	8.35	0.03396
0.90	0.10929	3.40	0.08904	5.90	0.01669	8.40	0.03604
0.95	0.05242	3.45	0.09113	5.95	0.00838	8.45	0.03720
1.00	0.00000	3.50	0.09095	6.00	0.00001	8.50	0.03745
1.05	0.04742	3.55	0.08856	6.05	0.00822	8.55	0.03677
1.10	0.08942	3.60	0.08410	6.10	0.01611	8.60	0.03521
1.15	0.12566	3.65	0.07771	6.15	0.02348	8.65	0.03280
1.20	0.15591	3.70	0.06961	6.20	0.03017	8.70	0.02961
1.25	0.18006	3.75	0.06003	6.25	0.03600	8.75	0.02573
1.30	0.19809	3.80	0.04925	6.30	0.04087	8.80	0.02127
1.35	0.21008	3.85	0.03755	6.35	0.04466	8.85	0.01634
1.40	0.21624	3.90	0.02523	6.40	0.04730	8.90	0.01107
1.45	0.21682	3.95	0.01262	6.45	0.04874	8.95	0.00558
1.50	0.21221	4.00	0.00001	6.50	0.04897	9.00	0.00001
1.55	0.20284	4.05	0.01223	6.55	0.04800	9.05	0.00549
1.60	0.18921	4.10	0.02395	6.60	0.04587	9.10	0.01079
1.65	0.17189	4.15	0.03481	6.65	0.04266	9.15	0.01578
1.70	0.15149	4.20	0.04454	6.70	0.03844	9.20	0.02032
1.75	0.12862	4.25	0.05295	6.75	0.03336	9.25	0.02432
1.80	0.10395	4.30	0.05988	6.80	0.02753	9.30	0.02765
1.85	0.07812	4.35	0.06519	6.85	0.02111	9.35	0.03033
1.90	0.05178	4.40	0.06880	6.90	0.01427	9.40	0.03220
1.95	0.02554	4.45	0.07065	6.95	0.00718	9.45	0.03327
2.00	0.00001	4.50	0.07074	7.00	0.00001	9.50	0.03351
2.05	0.02428	4.55	0.06910	7.05	0.00705	9.55	0.03292
2.10	0.04683	4.60	0.06582	7.10	0.01384	9.60	0.03154
2.15	0.06721	4.65	0.06100	7.15	0.02020	9.65	0.02940
2.20	0.08504	4.70	0.05480	7.20	0.02597	9.70	0.02656
2.25	0.10003	4.75	0.04740	7.25	0.03104	9.75	0.02310
2.30	0.11196	4.80	0.03899	7.30	0.03527	9.80	0.01910
2.35	0.12068	4.85	0.02981	7.35	0.03858	9.85	0.01468
2.40	0.12614	4.90	0.02009	7.40	0.04091	9.90	0.00995
2.45	0.12832	4.95	0.01007	7.45	0.04220	9.95	0.00502
2.50	0.12733	5.00	0.00001	7.50	0.04244	10.00	0.00002

(x) - B_o is the field at which the first zero occurs.

TABLE II

Circular junction, the field is normalized to the first minimum.

B/B_o	$I/I_1(0)$	B/B_o	$I/I_1(0)$	B/B_o	$I/I_1(0)$	B/B_o	$I/I_1(0)$
0.0	1.00000	2.05	0.05379	4.10	0.01771	6.15	0.01002
0.04	0.99692	2.09	0.05897	4.14	0.01437	6.19	0.01130
0.08	0.98771	2.13	0.06243	4.18	0.01079	6.23	0.01229
0.12	0.97250	2.17	0.06421	4.22	0.00705	6.27	0.01295
0.16	0.95146	2.21	0.06435	4.26	0.00324	6.31	0.01328
0.20	0.92485	2.25	0.06294	4.30	0.00054	6.35	0.01329
0.25	0.89300	2.30	0.06010	4.35	0.00419	6.40	0.01297
0.29	0.85630	2.34	0.05596	4.39	0.00765	6.44	0.01234
0.33	0.81518	2.38	0.05070	4.43	0.01082	6.48	0.01142
0.37	0.77014	2.42	0.04448	4.47	0.01364	6.52	0.01024
0.41	0.72170	2.46	0.03751	4.51	0.01605	6.56	0.00883
0.45	0.67045	2.50	0.02997	4.55	0.01801	6.60	0.00723
0.49	0.61696	2.54	0.02208	4.59	0.01948	6.64	0.00549
0.53	0.56186	2.58	0.01402	4.63	0.02044	6.68	0.00364
0.57	0.50574	2.62	0.00601	4.67	0.02088	6.72	0.00174
0.61	0.44923	2.66	0.00179	4.71	0.02079	6.76	0.00017
0.66	0.39294	2.71	0.00918	4.76	0.02021	6.81	0.00204
0.70	0.33745	2.75	0.01603	4.80	0.01914	6.85	0.00383
0.74	0.28332	2.79	0.02220	4.84	0.01764	6.89	0.00549
0.78	0.23107	2.83	0.02756	4.88	0.01575	6.93	0.00699
0.82	0.18119	2.87	0.03203	4.92	0.01352	6.97	0.00829
0.86	0.13412	2.91	0.03554	4.96	0.01102	7.01	0.00937
0.90	0.09024	2.95	0.03805	5.00	0.00831	7.05	0.01020
0.94	0.04988	2.99	0.03953	5.04	0.00547	7.09	0.01076
0.98	0.01331	3.03	0.04001	5.08	0.00256	7.13	0.01106
1.02	0.01928	3.07	0.03950	5.12	0.00035	7.17	0.01107
1.07	0.04772	3.12	0.03805	5.17	0.00317	7.21	0.01082
1.11	0.07196	3.16	0.03575	5.21	0.00585	7.26	0.01031
1.15	0.09197	3.20	0.03267	5.25	0.00833	7.30	0.00956
1.19	0.10779	3.24	0.02891	5.29	0.01054	7.34	0.00858
1.23	0.11954	3.28	0.02460	5.33	0.01245	7.38	0.00741
1.27	0.12736	3.32	0.01985	5.37	0.01401	7.42	0.00608
1.31	0.13148	3.36	0.01479	5.41	0.01520	7.46	0.00462
1.35	0.13213	3.40	0.00956	5.45	0.01599	7.50	0.00308
1.39	0.12961	3.44	0.00428	5.49	0.01637	7.54	0.00148
1.43	0.12426	3.48	0.00091	5.53	0.01635	7.58	0.00013
1.48	0.11640	3.53	0.00591	5.58	0.01592	7.62	0.00170
1.52	0.10643	3.57	0.01059	5.62	0.01512	7.67	0.00322
1.56	0.09471	3.61	0.01485	5.66	0.01397	7.71	0.00462
1.60	0.08165	3.65	0.01861	5.70	0.01250	7.75	0.00590
1.64	0.06761	3.69	0.02180	5.74	0.01076	7.79	0.00701
1.68	0.05298	3.73	0.02435	5.78	0.00880	7.83	0.00793
1.72	0.03813	3.77	0.02624	5.82	0.00666	7.87	0.00864
1.76	0.02339	3.81	0.02742	5.86	0.00440	7.91	0.00913
1.80	0.00910	3.85	0.02791	5.90	0.00208	7.95	0.00939
1.84	0.00448	3.89	0.02770	5.94	0.00024	7.99	0.00941
1.89	0.01707	3.94	0.02682	5.99	0.00250	8.03	0.00921
1.93	0.02845	3.98	0.02533	6.03	0.00466	8.08	0.00878
1.97	0.03846	4.02	0.02326	6.07	0.00666	8.12	0.00815
2.01	0.04694	4.06	0.02070	6.11	0.00846	8.16	0.00733